Journal of Thermal Analysis and Calorimetry
https://doi.org/10.1007/s10973-024-13346-7

Effect of using a ZnO-TiO_2/water hybrid nanofluid on heat transfer performance and pressure drop in a flat tube with louvered finned heat exchanger

Emre Askin Elibol[1] · Yunus Emre Gonulacar[2] · Fatih Aktas[2] · Burak Tigli[2]

Received: 7 March 2024 / Accepted: 24 May 2024
© The Author(s) 2024

Abstract

This study used an experimental setup consisting of a flat tube with a louvered finned crossflow configuration to examine the effects of utilizing a ZnO-TiO_2-water hybrid nanofluid on heat transfer rate, heat transfer coefficient, Nusselt number, and pressure drop. The studies were carried out under laminar flow conditions ($200 < Re < 800$), at four different temperatures (50, 60, 70, 80 °C), four different volume concentrations of nanoparticles (0.025, 0.05, 0.1, 0.2%), and three different volume flow rates (4, 6, 8 LPM). The findings were compared with pure water (0%). The results indicate that using hybrid nanofluid improves the heat transfer performance and increases pressure loss in comparison with pure water. When comparing hybrid nanofluid to pure water, the largest increases in heat transfer rate, heat transfer coefficient, Nusselt number, and pressure drop were 87.8%, 21.7%, 26.4%, and 10%, respectively. In addition, it was found that, up to a specific value (0.05%), increasing the nanoparticle volume concentration enhanced the heat transfer rate, heat transfer coefficient and Nusselt number, but which began to decrease on increasing the concentration past this value. Therefore, it was concluded that nanoparticle volume concentrations greater than 0.05% negatively affect heat transfer under the current operating conditions. The maximum heat transfer rate, heat transfer coefficient, and Nusselt number were obtained under the conditions of an 8 LPM volume flow rate, 80 °C inlet temperature, and 0.05% volume concentration.

Keywords Hybrid nanofluid · Heat exchanger · Flat tube · Louvered fin · ZnO · TiO_2

List of symbols

A_c	Cross-section area, m^2
A_s	Surface area, m^2
C_p	Specific heat, J kg^{-1} K^{-1}
D_h	Hydraulic diameter, m
f	Friction factor
F_d	Flow depth, m
F_h	Fin height, m
F_p	Fin pitch, m
h	Heat transfer coefficient, W m^{-2} K^{-1}
m	Mass, kg
$\dot{m}$	Mass flow rate, kg s^{-1}
Nu	Nusselt number
k	Thermal conductivity, W m^{-1} K^{-1}
L_α	Louver angle, m
L_h	Louver height, m
L_p	Louver pitch, m
P_w	Wetted perimeter
$\dot{Q}$	Heat transfer rate, W
Re	Reynolds number
S_1	Non-louvered inlet and exit fin length, m
S_2	Re-direction length, m
T	Temperature, °C
u	Inlet velocity, m s^{-1}
$\dot{V}$	Volume flow rate, LPM
$\dot{W}$	Pumping power, W

Greek symbols

φ	Volume concentration
ρ	Density, kg m^{-3}
μ	Dynamic viscosity, kg m^{-1} s^{-1}

Subscripts

b	Bulk
bf	Base fluid
hnf	Hybrid nanofluid

✉ Yunus Emre Gonulacar
yunusemre.gonulacar@gazi.edu.tr

[1] Department of Mechanical Engineering, Faculty of Engineering, Giresun University, Giresun, Türkiye

[2] Department of Mechanical Engineering, Faculty of Engineering, Gazi University, Ankara, Türkiye

Published online: 25 June 2024

in Inlet
np Nanoparticle
out Outlet
w Wall

Introduction

In many technical applications, including chemical processing, power systems, heat pumps, automotive, aerospace, and electronic chip cooling, heat exchanger systems are absolutely essential components [1]. Incompatible heat transfer mechanisms between the heat sources (or pool) and the fluid, decreasing efficiency with time, decreased heat transfer as a result of calcification, pressure loss, and pumping power consumption are common issues with such systems [2, 3]. The thermal performances of heat transfer fluids, including such substances as the water, oil, and ethylene glycol traditionally used in heat exchangers, are limited due to their relatively weak thermal properties, and these fluids need to be improved to solve the problems noted above [4]. Therefore, the research for highly efficient heat transfer fluids continues to date, with various researchers attempting to advance special classes of heat transfer fluids to increase thermal properties in recent years [5]. One obvious way to improve heat transfer is to add metallic materials to conventional heat transfer fluids. Over the past century, many studies have been conducted on adding millimeter- and micrometer-sized particles to conventional heat transfer fluids [4]. In these studies, although it was stated that the use of such additives showed considerable thermal improvement, it was also observed that some extreme problems, such as the increase in pressure drop, corrosion of pipelines, clogging of flow channels, and poor stability of the suspension, were experienced. Therefore, even though these fluids exhibit superior thermal performance over conventional heat transfer fluids, they are nevertheless unsuitable for use in actual heat transfer applications [5]. This has led both scientists and engineers to work on adjusting material properties at the nanoscale to increase the thermal performance of heat exchangers [6]. The advancement of nanotechnology has made it feasible to create particles with diameters of less than 100 nm [7]. "Nanofluids" are heat transfer fluids that are often created by distributing metallic or non-metallic nanoparticles in traditional heat transfer fluids that have an average diameter of less than 100 nm [2, 4]. The specific surface area of nanoscale particles is approximately 1000 times larger than the surface area of microscale particles since the size of solid particles in nanofluids is reduced, and their quantity per volume is increased. A greater surface area for heat transfer is provided by increasing the surface/volume ratio of the particles, which raises the rate of heat transfer [8–10]. In addition to improving heat transfer, the use of nanofluids allows for a reduction in the size and mass of the heat exchangers themselves [11]. Despite these stated advantages, the aggregation, agglomeration, and precipitation of nanoparticles over a certain volume ratio can restrict the heat transfer process in nanofluids, although it provides a significant increase in thermal conductivity [2]. Therefore, it is important to correctly determine the nanoparticle volume ratio correctly when using nanofluids. When the literature is examined, it can be seen that some researchers state that volume concentration is directly proportional to heat transfer, while others state that increasing volume concentration only positively affects heat transfer up to a certain value. In other words, the question of how nanoparticle volume concentration affects heat transfer is still not fully answered. In recent years, researchers have focused on theoretical and experimental analyses of hybrid nanofluids as well as mono-nanofluids [12]. Hybrid nanofluids are a novel type of nanofluid that consist of two or more nanoparticles combined at varying percentages for dispersal in the base liquid [13]. The main idea behind creating hybrid nanofluids is to improve properties such as mechanical resistance, thermal conductivity, physical strength, and chemical stability, compared to mono-nanofluids [14]. There are many studies in the literature in which various nanofluids have been used in different types of heat exchangers. Summaries of these studies are given in Table 1.

The literature research reveals that adding nanoparticles to a base liquid is beneficial in terms of heat transfer performance. Also, based on the literature, there is no study of which the authors are aware that considers the heat transfer performance of ZnO-TiO_2-water hybrid nanofluid in a flat tube heat exchanger, and it is observed that there is an inconsistency in terms of how heat transfer performance varies with increasing nanoparticle concentration. Therefore, in the current study, the aim was to examine the effects of different operating parameters on heat transfer and pressure drop in the flow of ZnO-TiO_2-water hybrid nanofluid in a flat-tube louvered-finned heat exchanger.

Experimental

Preparation of hybrid nanofluid

The SEM (scanning electron microscope) image of the TiO_2 and ZnO nanoparticles used in the study is given in Fig. 1. By importing the SEM image into the open-source program ImageJ, the average diameter of the nanoparticles was determined. First, the SEM images were calibrated using the established scale bar. To enable enough samples, the image's cleanest region was specifically chosen. Due to the contrast of the image, not every section of this region is excellent, meaning that thresholding has to be done by hand because

Table 1 Summaries of literature studies

Study	Nanofluid	φ/%	Heat exchanger	Flow regime	Results
Madhesh et al [2]	Cu–TiO_2-water	0.1–2	Tube-type counter flow	Transitional flow (3500 < Re < 7500)	Hybrid nanofluid increases h and Nu up to $\varphi = 0.1\%$
Kaska et al [15]	AlN-Al_2O_3-water	1–4	Straight horizontal flat tube	Turbulent flow (5000 < Re < 17,000)	Nu and ΔP increases with φ, but at more than 3% φ reduces the Nu
Madhesh and Kalaiselvam [16]	Cu-TiO_2-water	0.1–1	Tube-in-tube counter flow	Turbulent flow (4000 < Re < 15,000)	Maximum h is obtained at $\varphi = 0.7\%$
Suresh et al [17]	Al_2O_3-Cu-water	0.1	Straight circular tube	Laminar flow (Re < 2300)	Hybrid nanofluid increases the Nu and f compared to the base fluid
Sundar et al [18]	MWCNT-Fe_3O_4-water	0.1–0.3	Circular tube	Turbulent flow (3000 < Re < 22,000)	Nu, k, and f increase with hybrid nanofluid compared to the mono-nanofluids
Ahmed et al [19]	ZnO-TiO_2-Water	0.025–0.1 (mass)	Square	Turbulent flow (4550 < Re < 20,360)	Hybrid nanofluid increases the k, f, h and Nu compared to the base fluid
Huminic and Huminic [20]	GO-Co_3O_4-water	0.1–0.2	Flat, elliptical and circular duct	Laminar flow (100 < Re < 1000)	h increases with increases in both T_{in} and φ
Zhang et al [21]	TiO_2-water	0.005–1	Multi-port mini-channel flat tube	Transitional flow (100 < Re < 6100)	Nu increases with increasing φ at concentrations of less than 0.01%
Duangthongsuk and Wongwises[5]	TiO_2-water	0.2–2	Horizontal double-pipe counterflow	Turbulent flow (4500 < Re < 15,000)	h and Nu increase with increasing φ at concentrations of less than 1%
Ali et al [22]	ZnO-water	0.01–0.3	Car radiator	Turbulent flow (17,500 < Re < 27,600)	Nanofluid increases $\dot{Q}$ compared to the base fluid and provides a maximum $\dot{Q}$ at $\varphi = 0.2\%$
Qasım et al [23]	ZnO-water	0.1–0.3	Automobile radiator	Laminar flow (186 < Re < 1127)	$\dot{Q}$, h, and Nu increase with $\dot{V}$ and φ; after $\varphi = 0.2\%$, these values start to decrease. ΔP and f increase with increasing φ
Ali et al [24]	Al_2O_3-water	0.1–2	Car radiator	Laminar flow (100 < Re < 1000)	$\dot{Q}$, h and Nu reach their maximum values at $\varphi = 1\%$ and decrease for higher values
Tafakhori et al [9]	Fe_3O_4–water	0.01–0.9	Car radiator	Laminar flow (30 < Re < 100)	Nu increases until $\varphi = 0.1$ and then starts to decrease with φ. f and ΔP increase as φ increases
Sahin et al [4]	Al_2O_3-water	0.5–4	Circular tube	Turbulent flow (4000 < Re < 20,000)	Highest values of h and Nu are obtained at $\varphi = 1\%$. f increases with increasing φ

Table 1 (continued)

Study	Nanofluid	φ/%	Heat exchanger	Flow regime	Results
Yahya and Saghir [25]	Al_2O_3-water	1–2	Flat and circular pipe	Laminar flow (1000 < Re < 2000)	Nu is improved depending on the φ in the flat pipe flow. Flat pipe exhibits improved Nu compared to circular pipe
Safikhani and Abbasi [26]	Al_2O_3-water	0–3	Plain and flat tube	Laminar flow (100 < Re < 2000)	Use of nanofluid instead of base fluid and flat tubes improve Nu
Hussein et al [27]	TiO_2-water	1–2.5	Circular, elliptical and flat tube	Turbulent flow (5000 < Re < 20,000)	f and h increase with increasing φ. Flat tube has the highest h values
Hussein et al [28]	Al_2O_3-water TiO_2 -water SiO_2 -water	1–2.5	Flat and circular tube	Turbulent flow (5000 < Re < 50,000)	k, μ, f, and Nu increase with increasing φ. ΔP is lower in a flat tube than in a circular tube
She and Fan [29]	CuO-water	0.05–0.15	Flat and circular tube	Turbulent flow (6000 < Re < 10,000)	h and ΔP increase with increasing φ
Sharma et al [30]	CuO-water	0.1–0.5	Flat tube	Turbulent flow (3000 < Re < 9000)	Nu and ΔP increase with increasing φ and Re
Zhao et al [31]	Al_2O_3-water	1–6	Flat tube	Laminar flow (Re < 2300)	Nanofluid has higher h and ΔP than the base fluid
Sokhal et al [32]	CuO-water	0.1–0.5	Flat tube	Turbulent flow (5000 < Re < 20,000)	Nu and ΔP increase with increasing φ and Re
Alosious et al [33]	Al_2O_3-water CuO-water	0.05–1	Automobile radiator	Laminar flow (136 < Re < 816)	Increase in φ increases h, ε, and Ẇ. Optimum φ is between 0.4% and 0.8%
Vajjha et al [34]	Al_2O_3-EG/water CuO-EG/water	1–6	Automotive radiator	Turbulent flow (3000 < Re < 8000)	An increase in φ increases f and h

the particle boundaries are not always easily distinguished from one another. Consequently, 150 particles inside the outside bounds were manually chosen after the backdrop was erased to make just the particles visible, and the average diameter was computed using the area values.

The two-step method is the most widely utilized technique for preparation of nanofluids. The nanomaterials used in this process, such as nanoparticles, nanotubes, and nanofibers, are first made into dry powders using physical or chemical methods. In the second processing phase, high shear mixing, homogenization, ball milling, ultrasonic agitation, or intense magnetic force agitation are used to help disperse the nanosized powder into a liquid [33]. The preparation of the hybrid nanofluid used in the study is illustrated in Fig. 2, where beakers with a capacity of 2 L each were used to the 8-L nanofluid sample. Commercially purchased TiO_2 and ZnO nanoparticles were accurately weighed and added in equal proportions by mass (50:50) to 8 L of pure water to obtain the desired volume concentrations. Then, these fluids were mixed in a magnetic mixer (Mtops, 1500 rpm) for half an hour and then kept in an ultrasonic bath for 2 h. Triton X-100 surfactant was added to prevent sedimentation of the nanoparticles in the base fluid.

In order to see the stability of the hybrid nanofluids after they were prepared, the nanofluid samples with the highest concentration were kept for 2, 2.5, 3, and 4 h, as shown in Fig. 3, and no visible precipitation was observed at the end of the specified periods. This indicates that the nanofluid is stable.

The volume concentration of the hybrid nanofluid can be calculated using Eq. (1).

$$\varphi = \frac{\left(\frac{m}{\rho}\right)_{np1} + \left(\frac{m}{\rho}\right)_{np2}}{\left(\frac{m}{\rho}\right)_{np1} + \left(\frac{m}{\rho}\right)_{np2} + \left(\frac{m}{\rho}\right)_{bf}} \times 100 \quad (1)$$

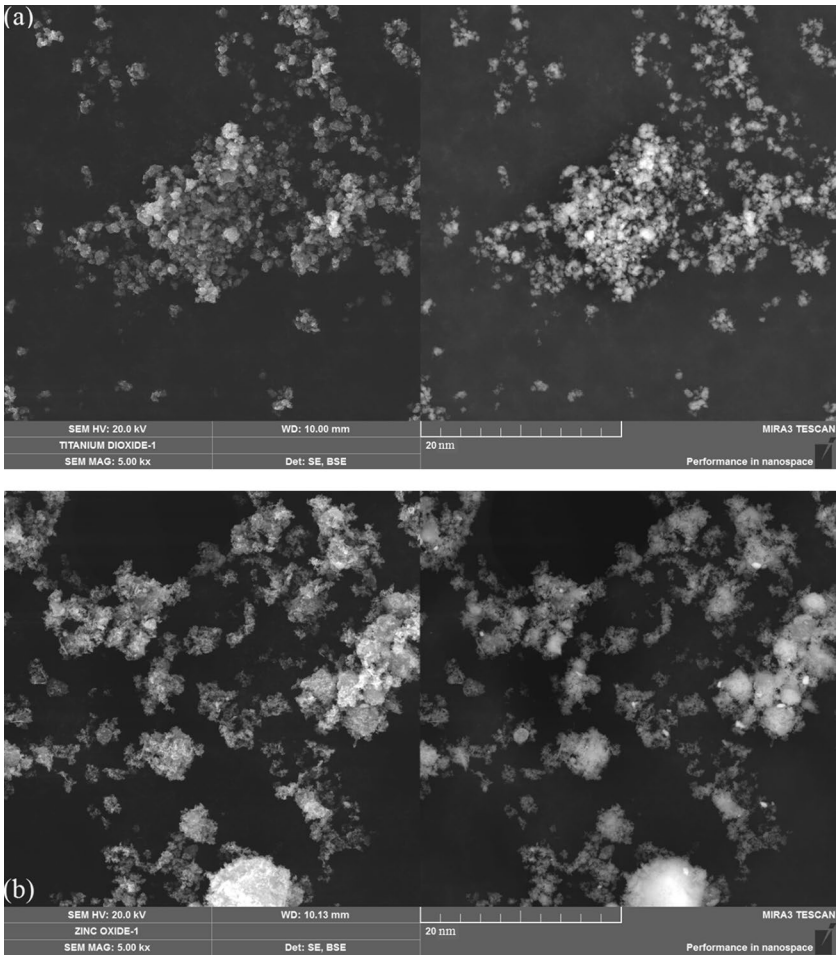


Fig. 1 SEM images of **a** TiO_2, and **b** ZnO nanoparticles

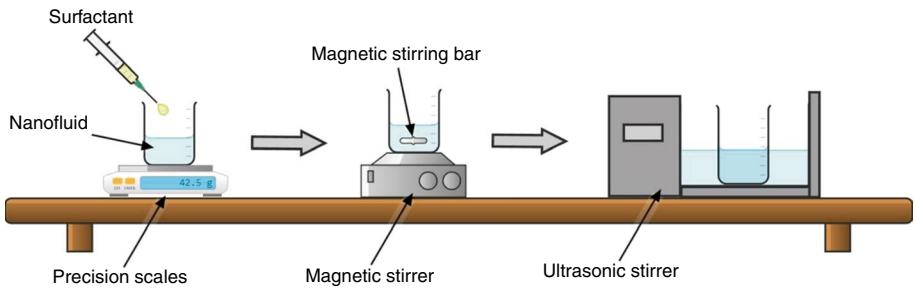


Fig. 2 Preparation of the hybrid nanofluid

Thermophysical properties of hybrid nanofluid

In heat transfer studies, the thermophysical properties of fluids have an important place in determining performance. Thermophysical properties of ZnO and TiO_2 nanoparticles are given in Table 2. The thermophysical properties of the hybrid nanofluid used in the study were found using the various correlations given below. While determining the thermophysical properties of the hybrid nanofluid, correlations that are widely used and verified in the literature [35–43] were

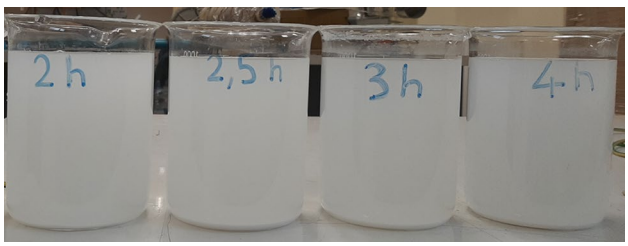


Fig. 3 Nanoparticle-water mixture for different waiting time

Table 2 Thermophysical properties of ZnO and TiO_2 nanoparticles [44]

Nanoparticles	ZnO	TiO_2
Density/kg m^{-3}	5500	4175
Specific heat capacity/J kg^{-1} K^{-1}	502.7	692
Thermal conductivity/W m^{-1} K^{-1}	58	8.4

preferred. The density (ρ_{hnf}) and the specific heat ($c_{p_{hnf}}$) of the ZnO-TiO_2-water hybrid nanofluid can be calculated via Eq. (2) and Eq. (3), respectively.

$$\rho_{hnf} = \rho_{bf}\left(1-\varphi_{np2}\right)\left[\left(1-\varphi_{np1}\right)+\varphi_{np1}\left(\frac{\rho_{np1}}{\rho_{bf}}\right)\right]+\varphi_{np2}\rho_{np2} \tag{2}$$

$$c_{phnf} = \frac{\rho_{bf}c_{pbf}\left(1-\varphi_{np2}\right)\left[\left(1-\varphi_{np1}\right)+\varphi_{np1}\frac{\rho_{np1}c_{pnp1}}{\rho_{bf}c_{pbf}}\right]+\varphi_{np2}\rho_{np2}c_{pnp2}}{\rho_{hnf}} \tag{3}$$

Here, φ_{np1}, φ_{np2}, ρ_{np1}, $\rho_{np2,}$ and ρ_{bf} indicate the volume concentration of the nanoparticles, and the densities of the nanoparticles and the base fluid, respectively. $c_{p_{np1}}$ and $c_{p_{np2}}$ are the specific heats of nanoparticles and $c_{p_{bf}}$ is the specific heat of the base fluid.

Thermal conductivity is the main thermophysical property determined for the fluids, and increasing the thermal conductivity compared to the base fluid is the main principle in the preparation of nanofluids. Calculation of the thermal conductivity of the ZnO-TiO_2-water hybrid nanofluid, k_{hnf}, is shown in Eq. (4).

$$k_{hnf} = k_{bf}\left[\frac{\frac{\varphi_{np1}k_{np1}+\varphi_{np2}k_{np2}}{\varphi}+2k_{bf}+2\left(\varphi_{np1}k_{np1}+\varphi_{np2}k_{np2}\right)-2\varphi k_{bf}}{\frac{\varphi_{np1}k_{np1}+\varphi_{np2}k_{np2}}{\varphi}+2k_{bf}-\left(\varphi_{np1}k_{np1}+\varphi_{np2}k_{np2}\right)+\varphi k_{bf}}\right] \tag{4}$$

where k_{np1}, k_{np2}, and k_{bf} indicate the thermal conductivities of the nanoparticles and base fluid, respectively.

Viscosity is another important indicator through which to evaluate the thermal properties of nanofluids [28]. The pressure drops caused by fluids and the pumping powers required to pump these fluids depend on the viscosity of the fluids. The dynamic viscosity of the hybrid nanofluid, μ_{hnf}, can be calculated via Eq. (5).

$$\mu_{hnf} = \mu_{bf}\left[1+32.795\varphi-7214\varphi^2+71400\varphi^3-\left(0.1941\times10^8\varphi^4\right)\right] \tag{5}$$

Here, φ is the total nanoparticle volume concentration, and can calculated via Eq. (6) or Eq. (1).

$$\varphi = \varphi_{np1}+\varphi_{np2} \tag{6}$$

Experimental setup and procedure

The experimental setup used in the study is illustrated in Fig. 4. The experimental setup consists of a heating tank, pump, turbine flowmeter, heat exchanger, snail fan, pressure gauge, thermocouples, and pipes. The heating tank, which has a volume of 30 l and has an electrical resistance, ensures that the fluid is maintained at the desired temperature. The pump, with three speed settings, circulates the fluid, and the stainless steel turbine flow meter is used to measure the volume flow rates. The nanofluid, which enters the heat exchanger hot, is returned to the heating tank by releasing its heat to the air when entering through the louvered fins. The heated air is evolved to the environment to be heated using a snail fan. As can be seen in Fig. 5, the heat exchanger used in the study has louvered fins, a flat tube, and a cross flow arrangement. In this figure, both louvered finned channels, through which air passes, and flat tubes, through which nanofluid passes, can be seen. A front view of flat tube inside

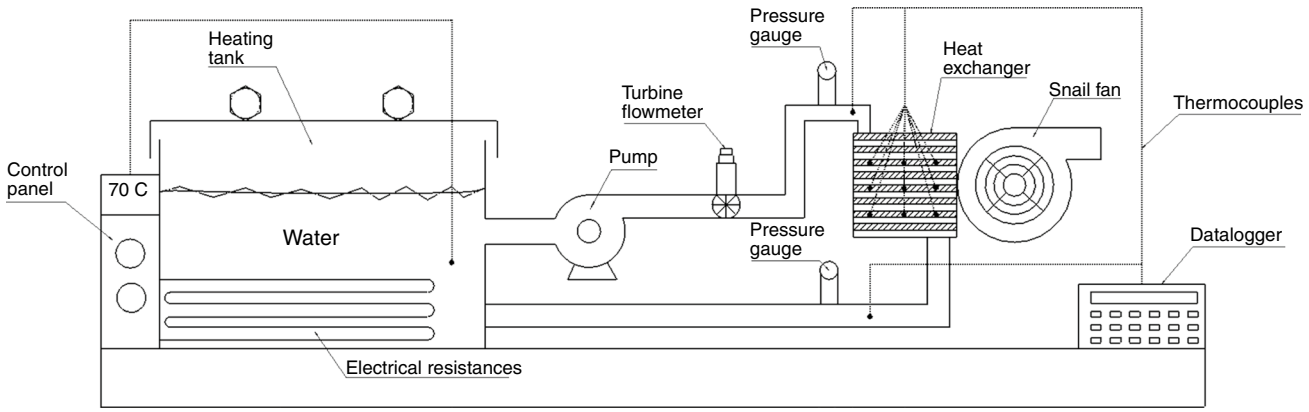


Fig. 4 Schematic view of the experimental setup

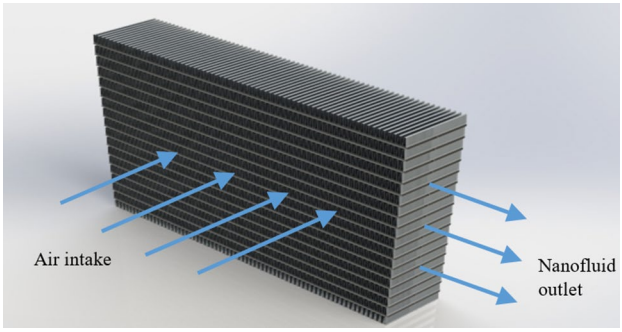


Fig. 5 The heat exchanger used in the study

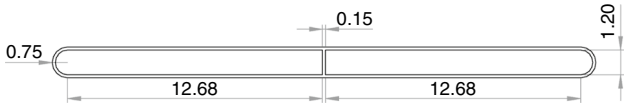


Fig. 6 Front view of flat tube inside the heat exchanger

the heat exchanger is given in Fig. 6. The unit for all geometric parameters presented in the figure is the millimeter. There are 17 flat tubes in the heat exchanger considered in this study. The cross-sectional view, front view, and geometric parameters of the louvered finned section through which the air passes are shown in Fig. 7 and reported in Table 3, respectively. Thermocouples and pressure gauges were positioned at the fluid's inlet and outlet points in the heat exchanger to measure the temperature and pressure. Additionally, as shown in Fig. 8, to determine the average wall temperature, the heat exchanger's back wall has nine T-type thermocouples fixed at various locations. Temperature readings are recorded via thermocouples coupled to a data logger. Every thermocouple that was employed in the studies was painstakingly calibrated in both boiling and ice water. The experimental setup was run for 7 min to keep the system steady. At ten-second intervals, the inlet and outlet pressure values, the inlet and outlet temperatures of the fluid,

Table 3 Geometric parameters of the louvered fin

Symbol	Value	Symbol	Value (mm)
S_1	1.4 mm	F_d	27
S_2	3.97 mm	F_p	0.98
L_p	0.6 mm	F_h	5
L_α	35°	L_h	4.22

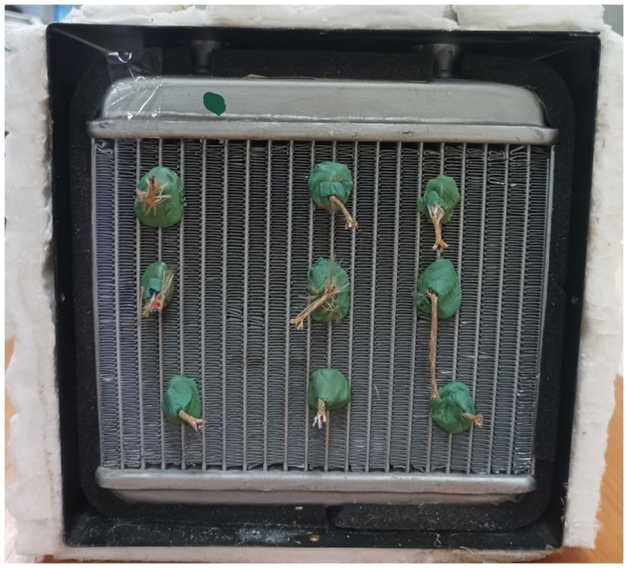


Fig. 8 Placement of thermocouples on the back wall of the heat exchanger

and the heat exchanger's wall temperatures were measured and their average values recorded. The average heat transfer rate, average heat transfer coefficient, and Nu number were calculated using these values. After the steady-state condition was reached, the measurement was repeated three times for reliability for each flow rate and inlet temperature at the volume concentration values examined.

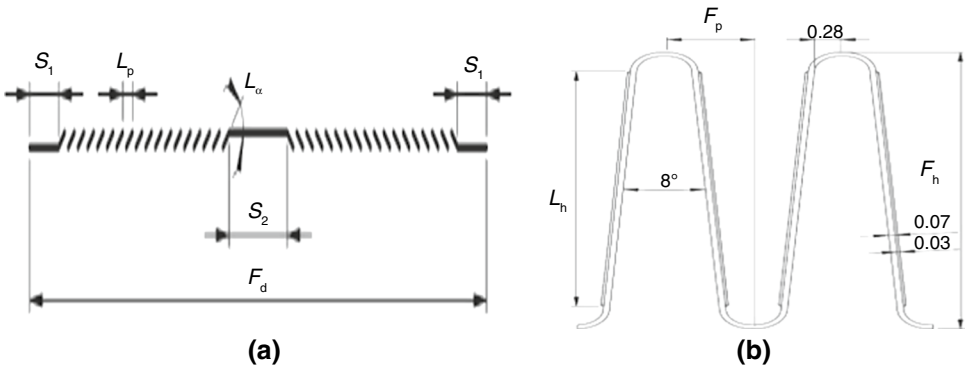


Fig. 7 Views of the louvered fin inside the heat exchanger: **a** cross-sectional view; and **b** front view

Table 4 Operating parameters

Parameters	Value
Inlet temperature of the nanofluid/°C	50, 60, 70, 80
Volume flow rate of the nanofluid/LPM	4, 6, 8
Volume concentration of nanoparticles/%	0.0025, 0.05, 0.1, 0.2
Air flow rate/LPM	2500

Within the scope of the study, the effects of a hybrid nanofluid flowing in a flat tube heat exchanger at different operating parameters on heat transfer rate, average heat transfer coefficient, Nu number, and pressure drop were investigated. The operating parameters are reported in Table 4. The heat exchanger used in the study is especially preferred for cabin heating system. The temperature of the coolant leaving the engine and entering the heater core can vary depending on the vehicle and operating conditions. The inlet temperatures in the current study are also found in the literature [45]. The pump used in the study has three different stages. Therefore, the flow rate was adjusted by changing the pump stage. In the experiments, the volume concentration was kept at low levels to prevent clumping, agglomeration, sedimentation, and pumping difficulties, whilst the flow rate of the air was kept constant at 2500 LPM.

To calculate the average heat transfer rate, average heat transfer coefficient, and average Nusselt number for the nanofluid side, a procedure can be followed. The heat transfer rate of the nanofluid is calculated using the conservation of mass and energy, as shown in Eq. (7).

$$\dot{Q} = \dot{m} c_{\mathrm{p}} \left(T_{\mathrm{in}} - T_{\mathrm{out}} \right) \tag{7}$$

The average heat transfer coefficient, h, is obtained as per Eq. (8):

$$h = \frac{\dot{Q}}{A_{\mathrm{s}} \left(T_{\mathrm{b}} - T_{\mathrm{w}} \right)} \tag{8}$$

where T_w is the wall temperature, T_b is the bulk temperature, and A_s is the surface area. The average wall temperature, T_w, in Eq. (8) is determined using the nine T-type thermocouples positioned at various points on the heat exchanger wall, as can be seen in Fig. 7. T_b is assumed to be the average values of the nanofluid's inlet and outlet temperatures across the heat exchanger, and is calculated as per Eq. (9):

$$T_{\mathrm{b}} = \frac{T_{\mathrm{in}} + T_{\mathrm{out}}}{2} \tag{9}$$

The average Nusselt number and Re number can be obtained from Eq. (10) and Eq. (11), respectively.

$$Nu = \frac{h D_{\mathrm{h}}}{k} \tag{10}$$

$$\mathrm{Re} = \frac{\rho u D_{\mathrm{h}}}{\mu} \tag{11}$$

where D_h is the total hydraulic diameter that can be calculated using Eq. (12).

$$D_{\mathrm{h}} = 4 A_{\mathrm{c}} / P_{\mathrm{w}} \tag{12}$$

where P_w is the wetted perimeter and A_c is the cross-sectional area.

With two pressure gauges connected at the inlet and outlet, the pressure drop on the nanofluid side of the heat exchanger can be computed as per Eq. (13):

$$\Delta P = P_{\mathrm{in}} - P_{\mathrm{out}} \tag{13}$$

Uncertainty analysis

To address the uncertainties arising from the instruments employed and the individuals or machines conducting the experiment, an uncertainty analysis can be performed according to the method initially introduced by Kline and McClintock [46]. This approach aims to analyze potential errors that may occur during the experiment and establish the reliability of the data so obtained. In this study, the primary factors contributing to uncertainty in experimental results are related to temperature measurements and the flow rate of the heat transfer fluid through the MCHSs.

If, in any experimental study, the magnitude to be calculated is denoted by R, and if n independent variables affecting this quantity are selected, then R can be expressed as follows:

$$R = \mathrm{f}\left(x_1, x_2, ..., x_{\mathrm{n}} \right) \tag{14}$$

When the fixed error amounts of each independent variable effective in the experiments are expressed as w_{x_1}, w_{x_2}, …, w_{x_n}, the amount of error in the calculation of R can be found as follows [47]:

$$W_{\mathrm{R}} = \left\{ \left(\frac{\partial R}{\partial x_1} w_1 \right)^2 + \left(\frac{\partial R}{\partial x_2} w_2 \right)^2 + ... + \left(\frac{\partial R}{\partial x_{\mathrm{n}}} w_{\mathrm{n}} \right)^2 \right\}^{1/2} \tag{15}$$

The maximum uncertainties of $\dot{Q}$, h, and Nu are approximately 3.6%, 4.2%, and %5.2, respectively.

Results and discussion

Experiments were carried out using four different inlet temperatures (50, 60, 70, 80 °C), three different volume flow rates (4, 6, and 8 LPM), and five different nanoparticle volume concentrations (0%, 0.0025%, 0.05%, 0.1%, and 0.2%); the effects of these parameters on heat transfer rate, heat transfer coefficient, Nu number, and pressure loss were examined. The findings are presented below under separate headings.

Heat transfer rate

For three different volume flow rates, the variation in heat transfer rates with volume concentration at various inlet temperatures is illustrated in Fig. 9. Examining the figure reveals that the heat transfer rate increases with the inlet temperature and volume flow rate. The heat transfer rate was enhanced by a maximum of 23% at 4 LPM and a maximum of 87% at 8 LPM when the inlet temperature increased from 50 to 80 °C for the same volume concentration. Figure 9 shows that the addition of nanoparticles to pure water increases the heat transfer rate. For all cases examined, the nanofluid's heat transfer rate was higher than that of pure water at any given temperature. Additionally, it can be seen from Fig. 9 that the heat transfer rate increases up to a 0.05% nanoparticle volume concentration but begins to decrease with increasing concentration beyond this point. This is due to the fact that when the volume concentration of nanoparticles increases, so do the nanofluid's density and viscosity. A denser and thicker boundary layer results from the high wall shear stress caused by the nanofluid's increased density and viscosity [16, 17]. Therefore, the heat transfer rate was negatively affected by the increase in concentration above 0.05% volume concentration. Since the flow regime in this study is laminar ($200 < Re < 800$), the flow depends more on viscosity than turbulent flow and the increase in viscosity is quite important. At relatively low volume concentrations, thermal conductivity dominates viscosity and enhances heat transfer. Because there are more particles in the base fluid at higher volume concentrations, there is a tendency for the particles to agglomerate and stability decreases. This instability causes the nanoparticles to

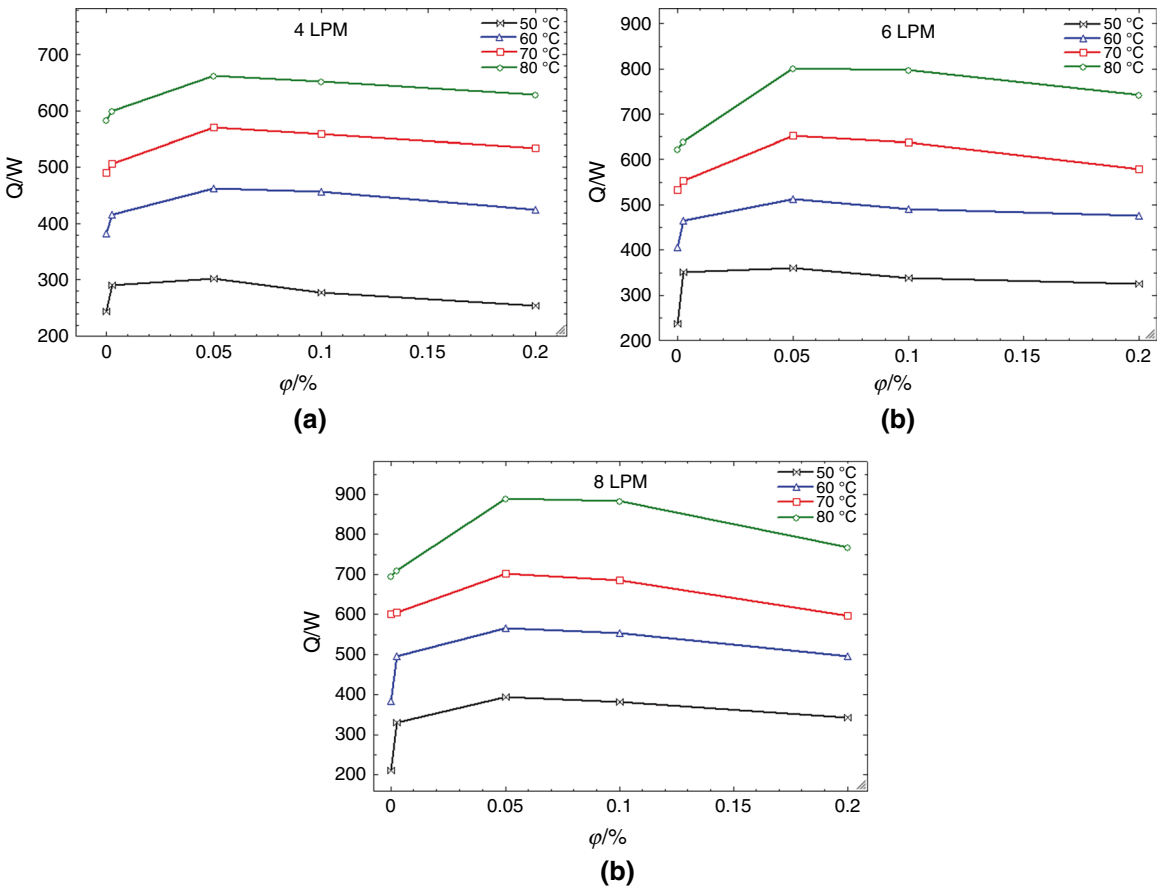


Fig. 9 Variation of heat transfer rates at different inlet temperatures according to volume concentration **a** 4 LPM, **b** 6 LPM, and **c** 8 LPM

precipitate. Above a certain concentration, the increase in viscosity begins to dominate the increase in thermal conductivity and reduces the heat transfer rate [48]. Similar results have been reported in various studies in the literature [4, 16, 17, 35]. In the current study, the highest heat transfer rates for all temperatures were obtained at 8 LPM and 0.05% concentration. The maximum heat transfer rates obtained for inlet temperatures of 50, 60, 70, and 80 °C are 395 W, 656 W, 701 W, and 889 W, respectively.

Heat transfer coefficient

Figure 10 illustrates the variation of the heat transfer coefficient depending on nanoparticle volume concentration and fluid inlet temperature according to different volume flow rates. From the figure, it can be observed that the heat transfer coefficient is enhanced with increasing fluid inlet temperature and volume flow rate at a given concentration. As shown in Fig. 10, the addition of nanoparticles to pure water increased the heat transfer coefficient. For all cases examined, the nanofluid's heat transfer coefficient was higher than that of pure water at a given temperature. The maximum increase in heat transfer coefficient with hybrid nanofluid compared to pure water was found to be 21.7%. For a volume flow rate of 4 LPM, the heat transfer coefficients obtained for $\varphi = 0\%$ and $\varphi = 0.0025\%$ at an inlet temperature of 50 °C were 355.5 W m^{-2} K^{-1} and 378.9 W m^{-2} K^{-1}, respectively, while when the inlet temperature increases to 80 °C, these values were determined to be 427.7 W m^{-2} K^{-1} and 438.6 W m^{-2} K^{-1}, respectively. Figure 10 shows that the heat transfer coefficient is enhanced up to a certain nanoparticle volume concentration (0.05%) and then decreases at all volume flow rates and inlet temperatures, as seen in the heat transfer rate. This is because adding nanoparticles to the base liquid simultaneously increases the viscosity and thermal conductivity of the base liquid, as explained in the heat transfer rate. The heat transfer performance increases with increasing thermal conductivity, while the heat transfer performance decreases with increasing fluid viscosity because it increases the thickness of the boundary layer. Consequently, the effect of increased heat conductivity can outweigh the effect of increased viscosity for volume concentrations of less than 0.05 vol%, while the opposite

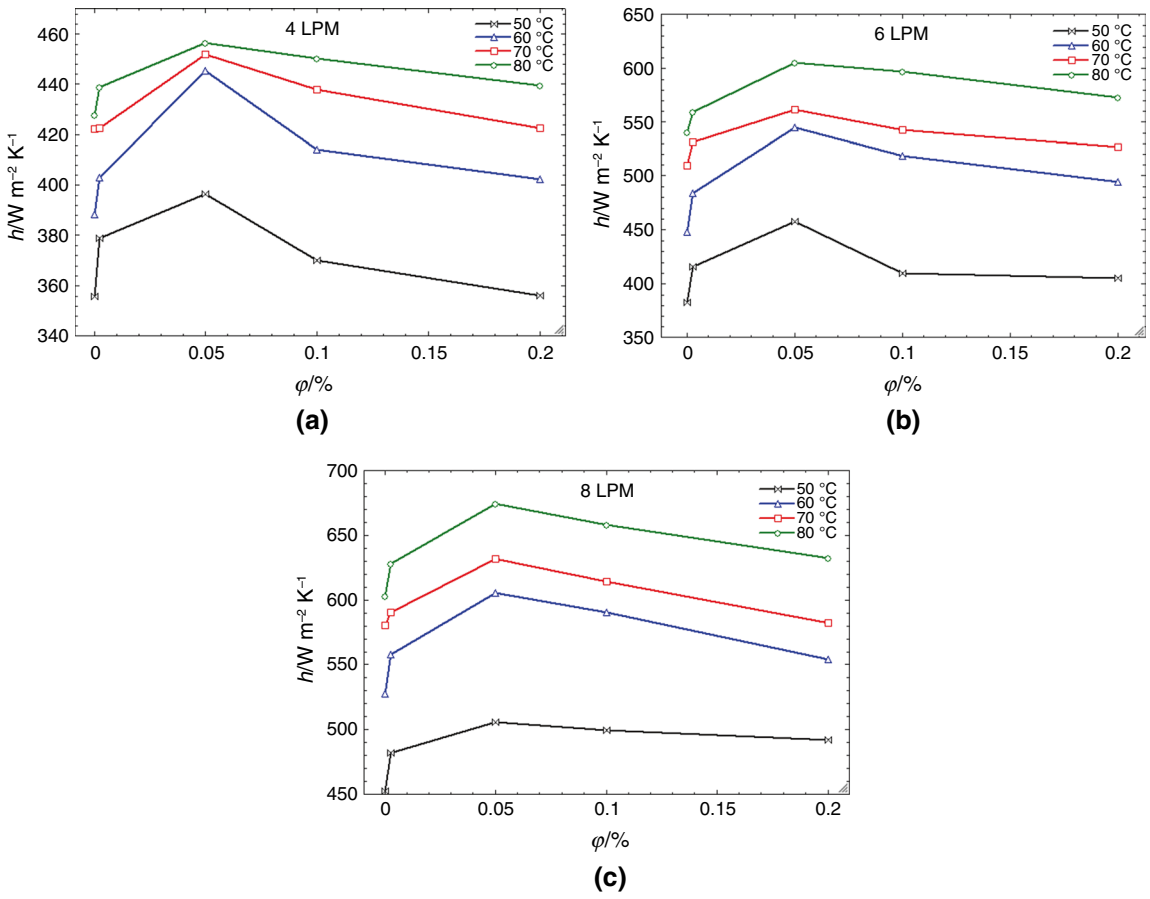


Fig. 10 Variation of heat transfer coefficients at different inlet temperatures according to volume concentration at **a** 4 LPM, **b** 6 LPM, and **c** 8 LPM

is true for volume concentrations greater than 0.05% [5]. In terms of heat transfer coefficient, there are other studies where a critical volume concentration of nanoparticles can be seen in the literature [2, 15, 17, 21, 35]. In the current study, the highest heat transfer coefficients for all temperatures were obtained at 8 LPM and a 0.05% concentration. The maximum heat transfer coefficients obtained for inlet temperatures of 50, 60, 70, and 80 °C were 506.1 W m^{-2} K^{-1}, 605.7 W m^{-2} K^{-1}, 631.8 W m^{-2} K^{-1}, and 674.5 W m^{-2} K^{-1}, respectively.

Nusselt number

Figure 11 shows the change in Nusselt number for three different volume flow rates at various volume concentrations and fluid inlet temperatures. When Fig. 11 is examined, it can be seen that the Nusselt number also increases with the increase in volumetric flow rate and fluid inlet temperature for a certain concentration, as in the heat transfer rate and heat transfer coefficient. Also, since a higher Nusselt number was obtained in all cases with the hybrid nanofluid compared to pure water, it can be said that the addition of nanoparticles to the base liquid increases the Nusselt number. The maximum increase in Nusselt number obtained with the hybrid nanofluid, as compared to the base fluid, is 26.4%. While the Nusselt numbers obtained for 0.1% and 0.2% volume concentrations at 4 LPM volume flow rate and 50 °C inlet temperature were 0.62 and 0.60, respectively, these values increased to 0.83 and 0.76, respectively, when the inlet temperature was increased to 80 °C. As the volume flow rate increased to 8 LPM, the Nusselt numbers obtained for 0.1% and 0.2% volume concentrations at a 50 °C inlet temperature were 0.88 and 0.87, respectively, which became 1.15 and 1.11, respectively, when the inlet temperature was increased to 80 °C. The figure shows that, like the situation observed for the heat transfer rate and heat transfer coefficient, the Nusselt number reaches a maximum at a 0.05% nanoparticle concentration at all inlet temperatures and volume flow rates and then begins to decrease. Because of the significant difference between the base fluid and the nanoparticle densities, nanoparticles usually cannot follow the velocity of the fluid and have a lower velocity. As in the current study, as the nanoparticle volume concentration increases at low speeds with no turbulence effect, it is possible that the probability of

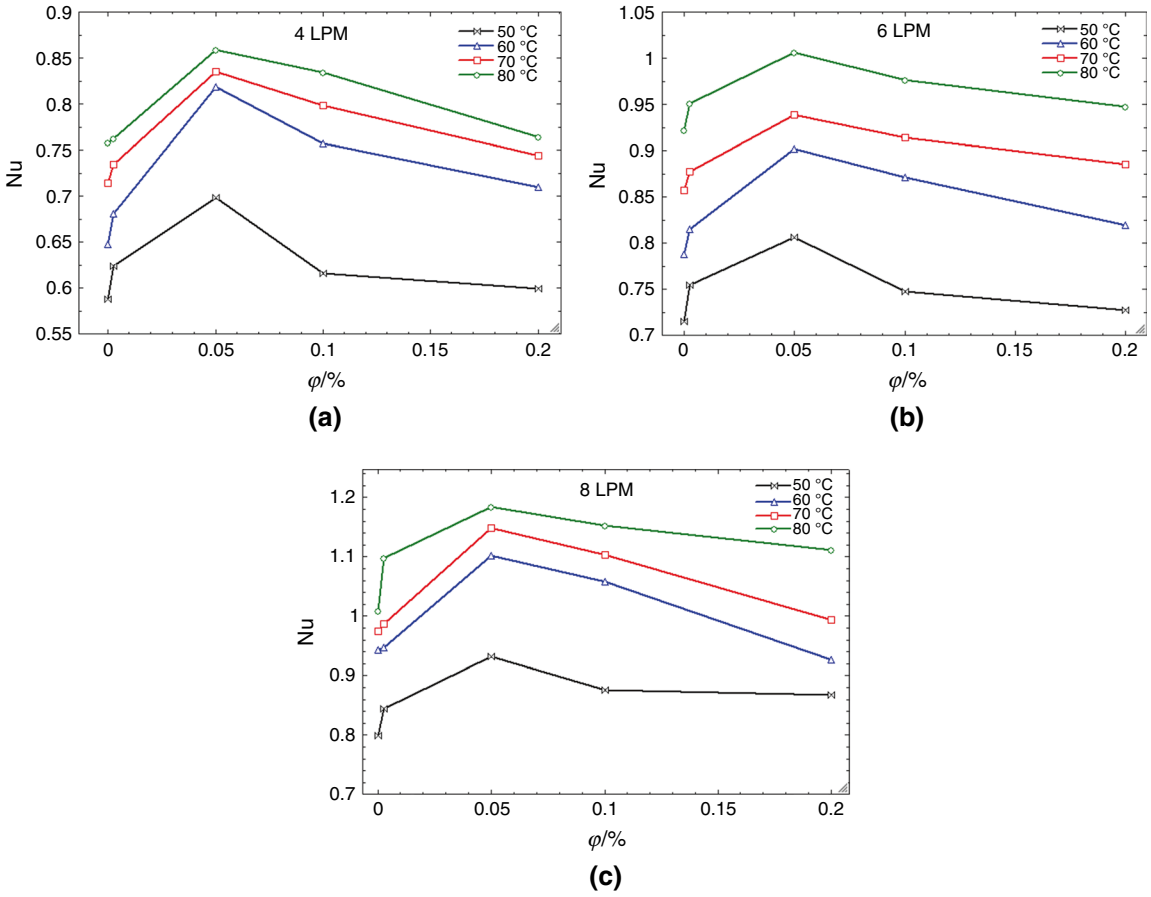


Fig. 11 Variation of Nusselt numbers according to volume concentration at different inlet temperatures: **a** 4 LPM, **b** 6 LPM, and **c** 8 LPM

nanoparticles agglomerating increases, the interlocking particles move more slowly as their effective diameter grows. This causes heat transfer to decrease at high nanoparticle concentrations [19, 35]. The critical value of the Nusselt number has been stated in other studies available in the literature [2, 14, 15, 17–19, 21, 35]. In the current study, the highest Nusselt numbers for all temperatures were obtained at 8 LPM and a 0.05% concentration. The maximum Nusselt numbers obtained for inlet temperatures of 50, 60, 70, and 80 °C were 0.93, 1.10, 1.15, and 1.18, respectively.

Figure 12 shows thermal camera images of the temperature distribution of the heat exchanger back surface at 4 LPM and 6 LPM for pure water and a 0.05% nanoparticle volume concentration at inlet temperatures of 70 °C and 80 °C. As can be seen in the figure, the maximum temperatures obtained for flow rates of 4 LPM and 6 LPM using pure water at an inlet temperature of 70 °C are 62 °C and 64 °C, respectively, while using the hybrid nanofluid with a 0.05% nanoparticle volume concentration gives temperatures of 63 °C and 65 °C, respectively. Similarly, using pure water at an inlet temperature of 80 °C, the maximum temperatures obtained for flow rates of 4 LPM and 6 LPM were 72 °C and 74 °C, respectively, while using the hybrid nanofluid with a 0.05% nanoparticle volume concentration gave temperatures of 73 °C and 75 °C, respectively. Therefore, it can be said that both the volume flow rate and temperature increase and the use of nanofluids positively affect the heat transfer performance because they increase the maximum temperature obtained on the back surface of the heat exchanger. Increasing the heat exchanger back surface temperature means that

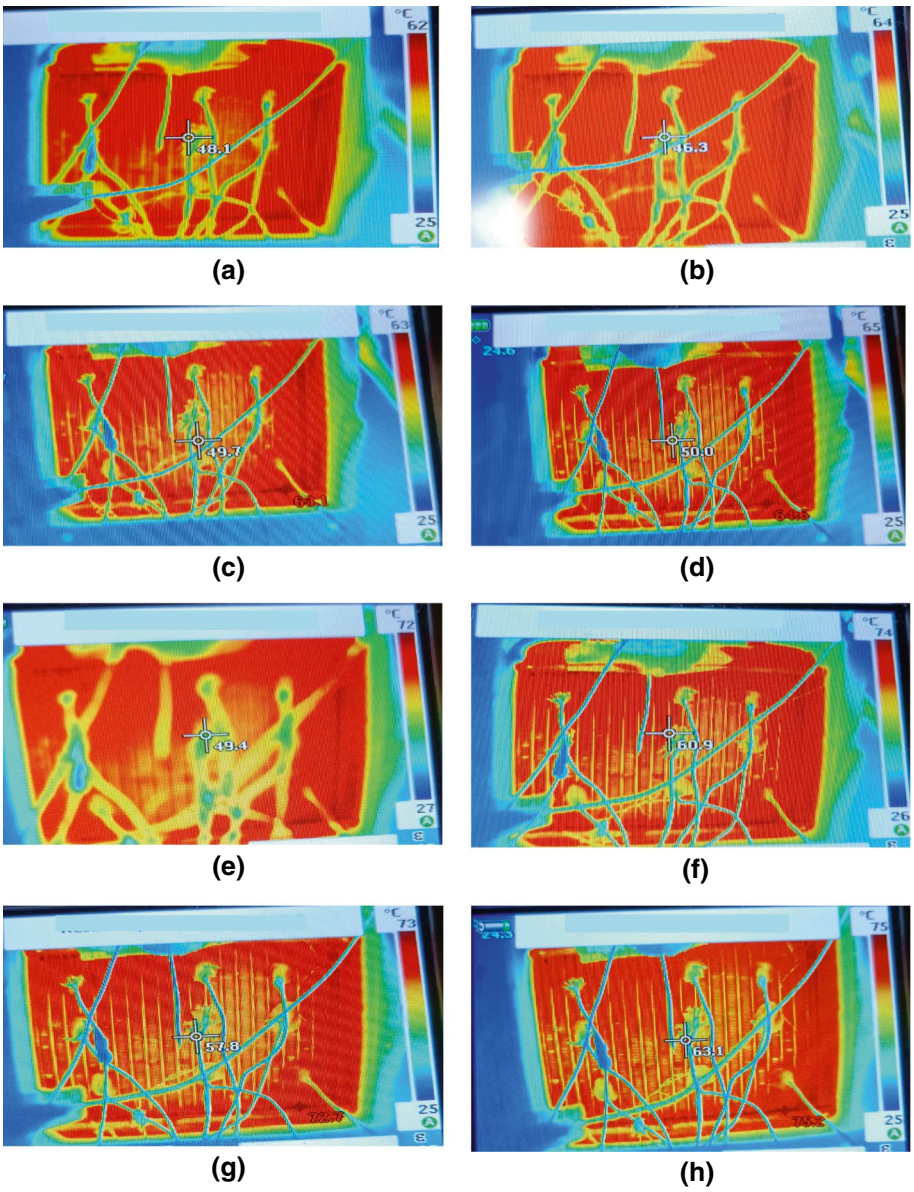


Fig. 12 Temperature distribution of the heat exchanger back surface: **a** 4 LPM, 70 °C, pure water, **b** 6 LPM, 70 °C, pure water, **c** 4 LPM, 70 °C, 0.05% ZnO-TiO_2-water, **d** 6 LPM, 70 °C, 0.05% ZnO-TiO_2-water, **e** 4 LPM, 80 °C, pure water, **f** 6 LPM, 80 °C, pure water, **g** 4 LPM, 80 °C, 0.05% ZnO-TiO_2-water, **h** 6 LPM, 80 °C, 0.05% ZnO-TiO_2-water

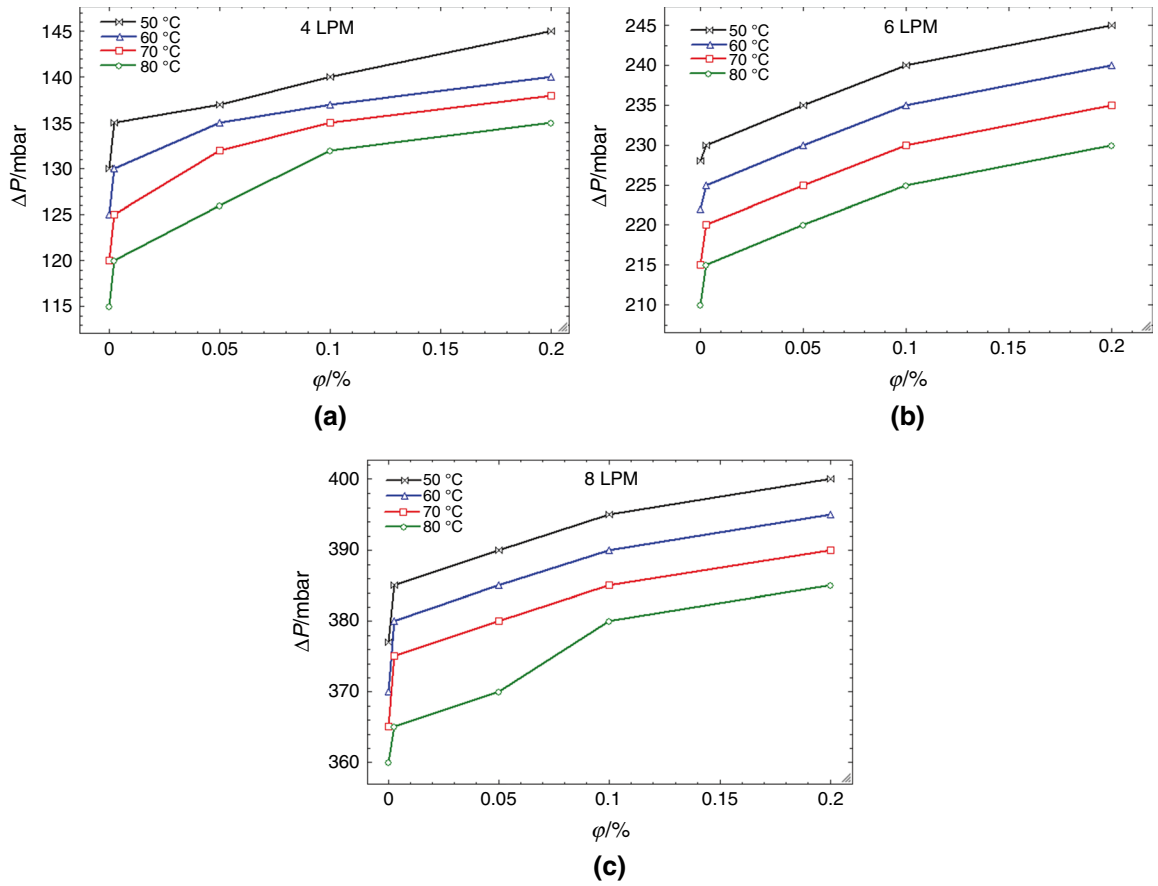


Fig. 13 Variation of pressure drop with inlet temperature and nanoparticle volume concentration at **a** 4 LPM, **b** 6 LPM, and **c** 8 LPM

the hot fluid entering the heat exchanger transfers its heat to the heat exchanger wall more quickly, and the temperature difference between the heat exchanger wall and the working fluid (T_b-T_w) decreases [48]. This causes the heat transfer performance to increase.

Pressure drop

Figure 13 shows pressure drop variation according to inlet temperature and nanoparticle volume concentration for three different volume flow rates. When Fig. 13 is examined, it can be seen that the pressure drop is inversely proportional to the inlet temperature and directly proportional to the volume flow rate. In the case of the 4 LPM flow rate and a 50 °C inlet temperature, the pressure drops obtained for pure water (0%) and a 0.0025% volume concentration are 130 mbar and 135 mbar, respectively, while these became 115 mbar and 120 mbar, respectively, on increasing the inlet temperature to 80 °C. In all cases examined, the addition of nanoparticles to pure water was found to increase the pressure drop. It has been observed that there is a maximum 10% increase in pressure drop with nanofluid compared to pure water. Additionally, it was observed that as the volume concentration of the nanoparticles increases, the pressure drop increases. These increases in pressure drop are due to the hybrid nanofluid having a higher viscosity and density than pure water due to the suspended ZnO-TiO_2 nanoparticles, thus resulting in greater friction during flow within the channel, and thus greater flow resistance. Moreover, the pressure drop of nanofluids is also significantly influenced by the Brownian motion, migration, fluctuation, dispersion, and flow pattern of the suspended ZnO-TiO_2 nanoparticles. These factors further increase the rates of momentum transfer between the nanoparticles, which in turn causes a higher pressure drop [23]. Therefore, for the reasons given above, both increasing nanoparticle volume concentration and the addition of nanoparticles to the base liquid increased the pressure drop.

Conclusions

In this study, the effects of the use of ZnO-TiO_2-water hybrid nanofluid on heat transfer rate, heat transfer coefficient, Nusselt number, and pressure drop under different operating

conditions in a flat tube louvered finned heat exchanger were experimentally examined. Experiments were carried out in a laminar flow regime using three different volume flow rates, four different inlet temperatures, and four different nanoparticle volume concentrations, the results of which were compared with those of pure water. The findings obtained as a result of the study are given below.

(1) As the inlet temperature and volume flow rate increase, the heat transfer rate also increases. Compared to pure water, the use of the nanofluid increases the heat transfer rate. The heat transfer rate is positively affected by an increase in concentration up to a certain point, after which it begins to decrease with increasing concentration.
(2) The heat transfer coefficient is directly proportional to the fluid inlet temperature and volume flow rate. The addition of nanoparticles to the base fluid increases the heat transfer coefficient. The heat transfer coefficient reaches a maximum at a 0.05% nanoparticle volume concentration in all cases, after which it then decreases.
(3) Nusselt number increases with increasing fluid inlet temperature and volume flow rate. Compared to pure water, the use of hybrid nanofluids positively affects the Nusselt number. Increasing the nanoparticle volume concentration up to a certain value increases the Nusselt number, after which it then decreases.
(4) Increasing the volume flow rate and decreasing the inlet temperature increases the pressure drop. Both the addition of nanoparticles to the base fluid and the increasing nanoparticle volume concentration result in an increase in pressure drop.
(5) In all cases examined, the maximum heat transfer rate, heat transfer coefficient, and Nusselt number were obtained at the highest volume flow rate, the highest inlet temperature, and a 0.05% nanoparticle concentration. Therefore, an 80 °C inlet temperature, 8 LPM volume flow rate, and 0.05% nanoparticle volume concentration are recommended as the optimum conditions for the current study.
(6) Therefore, this study has shown that using a hybrid nanofluid in this type of heat exchanger is promising in heat transfer.

The findings of this study may be informative for researchers considering the use of hybrid nanofluids in various heat exchangers in future. Additionally, the use of different hybrid nanofluids and higher fluid inlet temperatures and flow rates can be considered for future research.

Acknowledgments This work has been supported by the Gazi University Scientific Research Projects Coordination Unit under grant number FKB-2022-7523. We would like to thank them for their support. We would like to thank Prof. Dr. Oğuz TURGUT, Prof. Dr. Nuri YÜCEL, Prof. Dr. Hamit SOLMAZ, and Prof. Dr. Zeki YILMAZOĞLU, whose equipment we used during our studies. We would also like to express our gratitude to NURSAN Elektrik San. Tic. Ltd. Şti for their support in installing and repairing the experimental setup.

Funding Open access funding provided by the Scientific and Technological Research Council of Türkiye (TÜBİTAK).

Declarations

Conflict of interest The authors declare that they have no known competing financial interests or personal relationships that could have appeared to influence the work reported in this paper.

Open Access This article is licensed under a Creative Commons Attribution 4.0 International License, which permits use, sharing, adaptation, distribution and reproduction in any medium or format, as long as you give appropriate credit to the original author(s) and the source, provide a link to the Creative Commons licence, and indicate if changes were made. The images or other third party material in this article are included in the article's Creative Commons licence, unless indicated otherwise in a credit line to the material. If material is not included in the article's Creative Commons licence and your intended use is not permitted by statutory regulation or exceeds the permitted use, you will need to obtain permission directly from the copyright holder. To view a copy of this licence, visit http://creativecommons.org/licenses/by/4.0/.

References

1. Jiang H, Niu Y, Yang P, Liu Y. Effect of pulsation parameters on the spatial and temporal variation of flow and heat transfer characteristics in liquid metal cross flow the in-line tube bundle. Int J Heat Mass Transf. 2024;219:124871. https://doi.org/10.1016/j.ijheatmasstransfer.2023.124871.
2. Madhesh D, Parameshwaran R, Kalaiselvam S. Experimental investigation on convective heat transfer and rheological characteristics of Cu-TiO2 hybrid nanofluids. Exp Therm Fluid Sci. 2014;52:104–15. https://doi.org/10.1016/j.expthermflusci.2013.08.026.
3. Xu N, Liu Z, Yu X, Gao J, Chu H. Processes, models and the influencing factors for enhanced boiling heat transfer in porous structures. Renew Sustain Energy Rev. 2024;192:114244. https://doi.org/10.1016/j.rser.2023.114244.
4. Sahin B, Gültekin GG, Manay E, Karagoz S. Experimental investigation of heat transfer and pressure drop characteristics of Al2O3-water nanofluid. Exp Therm Fluid Sci. 2013;50:21–8. https://doi.org/10.1016/j.expthermflusci.2013.04.020.
5. Duangthongsuk W, Wongwises S. An experimental study on the heat transfer performance and pressure drop of TiO2-water nanofluids flowing under a turbulent flow regime. Int J Heat Mass Transf. 2010;53:334–44. https://doi.org/10.1016/j.ijheatmasstransfer.2009.09.024.
6. Çifţi E. Simulation of nucleate pool boiling heat transfer characteristics of the aqueous kaolin and bauxite nanofluids. Heat Transf Res. 2021;52:77–92.
7. Babar H, Wu H, Zhang W, Shah TR, McCluskey D, Zhou C. The promise of nanofluids: a bibliometric journey through advanced heat transfer fluids in heat exchanger tubes. Adv Colloid Interface Sci. 2024;325:103112. https://doi.org/10.1016/j.cis.2024.103112.
8. Cui Y, Tian S, Zoras S, Zhu J. Recent advances in various nanomaterials utilized in geothermal heat exchangers. Nano Energy. 2024;122:109309. https://doi.org/10.1016/j.nanoen.2024.109309.

9. Tafakhori M, Kalantari D, Biparva P, Peyghambarzadeh SM. Assessment of Fe3O4–water nanofluid for enhancing laminar convective heat transfer in a car radiator. J Therm Anal Calorim. 2021;146:841–53. https://doi.org/10.1007/s10973-020-10034-0.
10. Babat RAA, Martin K, Çiftçi E, Sözen A. Experimental study on the utilization of magnetic nanofluids in an air-to-air heat pipe heat exchanger. Chem Eng Commun. 2023;210:687–97. https://doi.org/10.1080/00986445.2021.1977634.
11. Sahoo RR, Sarkar J. Heat transfer performance characteristics of hybrid nanofluids as coolant in louvered fin automotive radiator. Heat Mass Transf und Stoffuebertragung. 2017;53:1923–31.
12. Asadi A, Alarifi IM, Foong LK. An experimental study on characterization, stability and dynamic viscosity of CuO-TiO2/water hybrid nanofluid. J Mol Liq. 2020. https://doi.org/10.1016/j.molliq.2020.112987.
13. Hormozi F, ZareNezhad B, Allahyar HR. An experimental investigation on the effects of surfactants on the thermal performance of hybrid nanofluids in helical coil heat exchangers. Int Commun Heat Mass Transf. 2016;78:271–6. https://doi.org/10.1016/j.icheatmasstransfer.2016.09.022.
14. Hemmat Esfe M, Abbasian Arani AA, Rezaie M, Yan WM, Karimipour A. Experimental determination of thermal conductivity and dynamic viscosity of Ag-MgO/water hybrid nanofluid. Int Commun Heat Mass Transf. 2015;66:189–95. https://doi.org/10.1016/j.icheatmasstransfer.2015.06.003.
15. Kaska SA, Khalefa RA, Hussein AM. Hybrid nano fluid to enhance heat transfer under turbulent fl ow in a flat tube. Case Stud Therm Eng. 2019;13:4–13.
16. Madhesh D, Kalaiselvam S. Experimental analysis of hybrid nanofluid as a coolant. Procedia Eng. 2014;97:1667–75. https://doi.org/10.1016/j.proeng.2014.12.317.
17. Suresh S, Venkitaraj KP, Selvakumar P, Chandrasekar M. Effect of Al 2O 3-Cu/water hybrid nanofluid in heat transfer. Exp Therm Fluid Sci. 2012;38:54–60. https://doi.org/10.1016/j.expthermflusci.2011.11.007.
18. Sundar LS, Singh MK, Sousa ACM. Enhanced heat transfer and friction factor of MWCNT-Fe3O4/water hybrid nanofluids. Int Commun Heat Mass Transf. 2014;52:73–83. https://doi.org/10.1016/j.icheatmasstransfer.2014.01.012.
19. Ahmed W, Kazi SN, Chowdhury ZZ, Johan MR. One-pot sonochemical synthesis route for the synthesis of ZnO@TiO2/DW hybrid/composite nanofluid for enhancement of heat transfer in a square heat exchanger. J Therm Anal Calorim. 2021;143:1139–55. https://doi.org/10.1007/s10973-020-09362-y.
20. Huminic G, Huminic A. A numerical approach on hybrid nanofluid behavior in laminar duct flow with various cross sections. J Therm Anal Calorim. 2020;140:2097–110. https://doi.org/10.1007/s10973-019-08990-3.
21. Zhang J, Diao Y, Zhao Y, Zhang Y. Experimental study of TiO2-water nanofluid flow and heat transfer characteristics in a multiport minichannel flat tube. Int J Heat Mass Transf. 2014;79:628–38. https://doi.org/10.1016/j.ijheatmasstransfer.2014.08.071.
22. Ali HM, Ali H, Liaquat H, Bin Maqsood HT, Nadir MA. Experimental investigation of convective heat transfer augmentation for car radiator using ZnO-water nanofluids. Energy. 2015;84:317–24.
23. Qasim M, Sajid Kamran M, Ammar M, Ali Jamal M, Yasar JM. Heat transfer enhancement of an automobile engine radiator using ZnO water base nanofluids. J Therm Sci. 2020;29:1010–24.
24. Ali M, El-Leathy AM, Al-Sofyany Z. The effect of nanofluid concentration on the cooling system of vehicles radiator. Adv Mech Eng. 2014;2014:1–13.
25. Yahya M, Saghir MZ. Thermal analysis of flow in a porous flat tube in the presence of a nanofluid: Numerical approach. Int J Thermofluids. 2021. https://doi.org/10.1016/j.apt.2015.09.002.
26. Safikhani H, Abbasi F. Numerical study of nanofluid flow in flat tubes fitted with multiple twisted tapes. Adv Powder Technol. 2015;26:1609–17. https://doi.org/10.1016/j.apt.2015.09.002.
27. Hussein AM, Sharma KV, Bakar RA, Kadirgama K. The effect of cross sectional area of tube on friction factor and heat transfer nanofluid turbulent flow. Int Commun Heat Mass Transf. 2013;47:49–55. https://doi.org/10.1016/j.icheatmasstransfer.2013.06.007.
28. Hussein AM, Sharma KV, Bakar RA, Kadirgama K. The effect of nanofluid volume concentration on heat transfer and friction factor inside a horizontal tube. J Nanomater. 2013;2013:1–12.
29. She L, Fan G. Numerical simulation of flow and heat transfer characteristics of CuO-water nanofluids in a flat tube. Front Energy Res. 2018;6:1–8.
30. Sharma P, Kumar V, Sokhal GS, Dasaroju G, Bulasara VK. Numerical study on performance of flat tube with water based copper oxide nanofluids. Mater Today Proc. 2020;21:1800–8. https://doi.org/10.1016/j.matpr.2020.01.234.
31. Zhao N, Yang J, Li H, Zhang Z, Li S. Numerical investigations of laminar heat transfer and flow performance of Al2O3-water nanofluids in a flat tube. Int J Heat Mass Transf. 2016;92:268–82. https://doi.org/10.1016/j.ijheatmasstransfer.2015.08.098.
32. Singh Sokhal G, Gangacharyulu D, Bulasara VK. Influence of copper oxide nanoparticles on the thermophysical properties and performance of flat tube of vehicle cooling system. Vacuum. 2018;157:268–76. https://doi.org/10.1016/j.vacuum.2018.08.048.
33. Alosious S, Sarath R, Nair AR, Krishnakumar K. Experimental and numerical study on heat transfer enhancement of flat tube radiator using Al2O3 and CuO nanofluids. Heat Mass Transf. 2017;53:3545–63.
34. Vajjha RS, Das DK, Ray DR. Development of new correlations for the Nusselt number and the friction factor under turbulent flow of nanofluids in flat tubes. Int J Heat Mass Transf. 2015;80:353–67. https://doi.org/10.1016/j.ijheatmasstransfer.2014.09.018.
35. Ghadikolaei SS, Yassari M, Sadeghi H, Hosseinzadeh K, Ganji DD. Investigation on thermophysical properties of Tio 2—Cu / H 2 O hybrid nano fl uid transport dependent on shape factor in MHD stagnation point fl ow. Powder Technol. 2017;322:428–38. https://doi.org/10.1016/j.powtec.2017.09.006.
36. Mansouri R, Pourrajab R, Behbahani M, Daneh-Dezfuli A. Evaluating the convective heat transfer of graphene oxide–gold hybrid nanofluid flow in CPU. J Therm Anal Calorim. 2023;148:5765–76. https://doi.org/10.1007/s10973-023-12064-w.
37. Hyder A, Lim YJ, Khan I, Shafie S. Investigating heat transfer characteristics in nanofluid and hybrid nanofluid across melting stretching/shrinking boundaries. Bionanoscience. 2024. https://doi.org/10.1007/s12668-024-01309-z.
38. Mishra A, Pathak G. A comparative analysis of MoS2-SiO2/H2O hybrid nanofluid and MoS2-SiO2-GO/H2O ternary hybrid nanofluid over an inclined cylinder with heat generation/absorption. Numer Heat Transf Part A Appl. 2023. https://doi.org/10.1080/10407782.2023.2228483.
39. You X, Wang Y. Series solutions of three-dimensional magnetohydrodynamic hybrid nanofluid flow and heat transfer. Nanomaterials. 2024. https://doi.org/10.3390/nano14030316.
40. Tlili I. Impact of thermal conductivity on the thermophysical properties and rheological behavior of nanofluid and hybrid nanofluid. Math Sci. 2021. https://doi.org/10.1007/s40096-021-00377-6.
41. Chung JD, Ramzan M, Gul H, Gul N, Kadry S, Chu YM. Partially ionized hybrid nanofluid flow with thermal stratification. J Mater Res Technol. 2021;11:1457–68. https://doi.org/10.1016/j.jmrt.2021.01.095.
42. Subhani M, Nadeem S. Numerical analysis of micropolar hybrid nanofluid. Appl Nanosci. 2019;9:447–59. https://doi.org/10.1007/s13204-018-0926-2.

43. Gangadhar K, Bhargavi DN, Kannan T, Venkata Subba Rao M, Chamkha AJ. Transverse MHD flow of Al2O3-Cu/H2O hybrid nanofluid with active radiation: a novel hybrid model. Math Methods Appl Sci. 2020. https://doi.org/10.1002/mma.6671.
44. Pak BC, Cho YI. Hydrodynamic and heat transfer study of dispersed fluids with submicron metallic oxide particles. Exp Heat Transf. 1998;11:151–70.
45. Bhaiyat TI, Schekman S, Lim HY, Jeon YH, Kim T. Off-design performance of a louvered fin-tube heater core in an automotive climate control system. Appl Therm Eng. 2019;161:114155. https://doi.org/10.1016/j.applthermaleng.2019.114155.
46. Kline SJ, McClintock FA. Describing uncertainties in single-sample experiments. Mech Eng. 1953;75:3–8.
47. Holman J. Experimental methods for engineers. Notes Queries. 2011. https://doi.org/10.1061/TACEAT.0005571.
48. Elibol EA, Turgut O, Aktas F, Senol H, Celik AF. Experimental investigation on heat transfer and flow characteristics of TiO2-water nanofluid in a heavy vehicle radiator. J Therm Anal Calorim. 2023;148:977–94. https://doi.org/10.1007/s10973-022-11817-3.

Publisher's Note Springer Nature remains neutral with regard to jurisdictional claims in published maps and institutional affiliations.